

deepCR-ACS/WFC: Cosmic-Ray Rejection Model for HST ACS/WFC Photometry

K.J. KWON^{1,2}

¹*Department of Astronomy, University of California, Berkeley, CA 94720-3411, USA*

²*Department of Physics, University of California, Berkeley, CA 94720-3411, USA*

Submitted to Department of Astronomy, UC Berkeley

ABSTRACT

Cosmic-ray (CR) identification is an essential component in the observational data processing. DEEPCR (Zhang & Bloom 2020) is a deep-learning-based pipeline for cosmic-ray rejection and replacement, which demonstrates superior performance in CR detection over the best-in-class solution, LACOSMIC. DEEPCR was originally trained with Hubble Space Telescope (HST) ACS/WFC F606W images of 3 different fields – globular clusters, extragalactic fields, resolved galaxies. To provide full optical band coverage for HST ACS/WFC, we construct a training set that comprises images from F435W, F606W, and F814W filters and train both the individual filter models and all-in-one *global* model. We demonstrate supreme CR detection ability, providing near 100% true-positive rate (TPR) in globular clusters and extragalactic fields, and $\sim 90\%$ TPR in resolved galaxies.

Keywords: instrumentation: detectors – methods: data analysis – techniques: image processing

1. INTRODUCTION

Cosmic-ray (CR) contamination of observational images is caused by high-energy charged particles landing on detecting devices. As well as other space-based detectors, Hubble Space Telescope (HST) suffers cosmic-ray contamination, originating from various sources, including the radiation belt of the Earth. When the CR lands on detectors (the charged coupled devices, for example), the contaminated pixels accumulate significant quantities of charge resulting in abnormally high pixel values in images. Understanding the effect of CR contamination perhaps would be easier seen than read; Figure 1 shows the effect of CRs on HST ACS/WFC photometry images. As illustrated, the pixels affected by CRs are identifiable with abruptly high pixel values. However, the differentiability of CRs against *normal* astronomical objects varies between the images, with the most densely populated images being the hardest.

Resolving CRs against normal sources can be achieved by various means. One of the most fundamental methods is combining multiple exposures taken on the same field to generate median images (Fruchter & Hook 2002). Unlike sporadic arrival of CRs onto CCDs, the source objects in most of the images, such as stars or galaxies, are relatively stationary. In other words, if multiple exposures are available, the source objects are consistently present throughout the exposures in contrast to transient artifacts of CRs. With proper alignment, combining multiple exposures produces the CR-free median images, which can be used to create CR masks. Space Science Telescope Science Institution (STScI) provides an open-source python package which comprises modules—TWEAKREG (Gonzaga & et al. 2012) and ASTRODRIZZLE (Hack et al. 2012)—to align and combine images. The former module recognizes the common sources to align multiple exposure images, where the latter creates median images to create CR masks. However, this method cannot be utilized for a single exposure image since the median CR-free image cannot be created. In addition, if the sources of interest are transient or variable, or if the CCD read-out times are non-negligible, using multiple exposures is likely to deteriorate the quality of observation or entail high computational cost.

As an alternative, multiple methods have been proposed to process single exposure, which include image restoration technique (Freudling 1995), linear filtering (Rhoads 2000), histogram analysis (Pych 2004), and Laplacian-edge

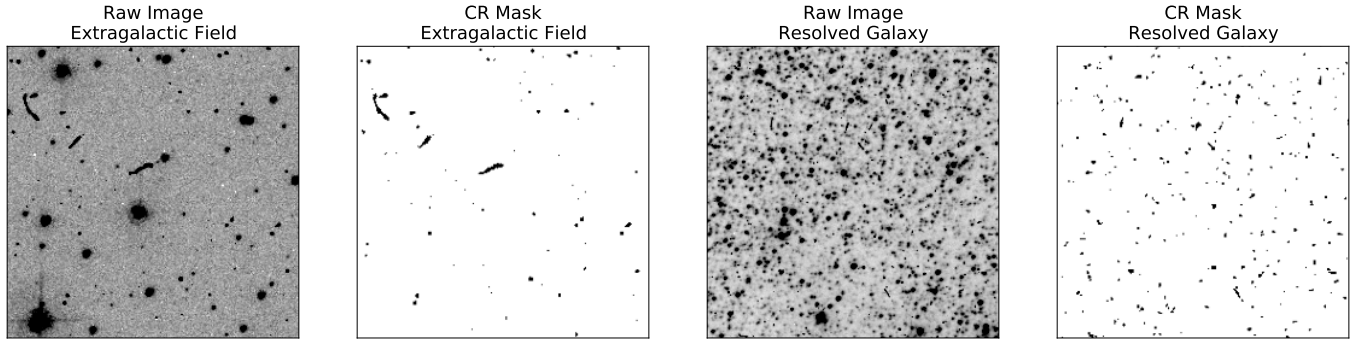


Figure 1. The first and the third panels show the raw images from HST ACS/WFC F435W, F606W observation, respectively. Shown in the second and the third panels are the CR masks generated by ASTRODRIZZLE. The field types are given in the titles. As explicated in the first paragraph in Section 1, the right image is more densely populated with astronomical sources, and the CRs are more difficult to resolve.

detection (van Dokkum 2001). Demonstrated by Farage & Pimbblet (2005) as a current best solution, LACOSMIC (van Dokkum 2001) utilizes Laplacian edge detection method to detect CRs from normal objects. The algorithm identifies and differentiates CRs from sources by their sharpness of edges, which makes it possible to identify CRs in a single exposure image. However, the computational cost necessary to process an image remains non-negligible, which urges the need for an efficient framework to process single exposure.

Recently developed DEEPCR (Zhang & Bloom 2020) is a deep-learning-based neural net pipeline for CR identification/replacement. Motivated by the aforementioned fact that the difficulty of identifying CRs varies with the type of fields, the training and test datasets were constructed with the images from extragalactic fields, globular clusters, and resolved galaxies, where all the images were taken with HST ACS/WFC F606W filter. The model demonstrated superior CR detection rate over LACOSMIC, with true positive rates (TPR) of 98.7%, 99.5% and 91.2%, respectively in the extragalactic field, globular cluster, resolved galaxy test images. Furthermore, the model outperforms LACOSMIC in speed; with GPU support, the model achieves $90\times$ speed boost compared with LACOSMIC. Although the model is anticipated to maintain its performance in lower/higher wavelength filters, we further consolidate the anticipation by training the models with the images taken with HST ACS/WFC F435W, F606W, F814W filters. We proceed in the same way as in Zhang & Bloom (2020) to construct training and test datasets. Then, we train the individual model for each filter and one *all-in-one* global model. In this paper, we demonstrate that all the four models retain the superior performance over LACOSMIC, and further show that the global model is a sufficient substitute for individual filter models. We defer reader to Zhang & Bloom (2020) for additional information in the model architecture.

2. DATA

We constructed the training dataset in the same manner as Zhang & Bloom (2020). The full list of the observation sets that were used in the training set is given in Table 1. For globular clusters and resolved galaxies, we queried the identifiers of famous objects such as M3 or M3. Then, datasets were constituted by close-up and distant views of the various parts of the queried objects. For the extragalactic field, we entered random coordinates and selected images that are classified as PARALLEL-FIELD or ANY and have significantly visible detector artifact. In total, 39 observation sets were selected, where each observation set consists of 2–8 exposure data. The individual models were trained with the observation sets that were taken with corresponding filters, and the global model was trained with the entire training set. The training dataset comprises the images, data quality arrays, and true CR masks of every exposure.

The images are directly taken from single-frame exposure files (**flc.fits*). Also, the training images were selected to train the model on three different fields, extragalactic field, globular cluster, resolved galaxies, where the difficulty to resolve CRs against normal sources ascends in the same order. The models are trained simultaneously on the three fields but were tested separately to assess their performance in each field. We deploy batch training by segmenting the original images into smaller patches of dimension 256×256 . To prevent the artifacts at the edges of the images from deteriorating the training outcome, we discard the first 128 pixels from the image boundary. Additionally, the images of which exposure time is shorter than 100 seconds were thrown out.

Table 1. HST ACS/WFC training dataset: 39 observation sets in total were used to train DEEPCR-ACS/WFC and DEEPCR-ACS/WFC F435W, F606W, F814W models. As shown, the training sets for individual models consist of images from 3 different fields.

Filter	Proposal ID	Observation set ID*	Field Type	N_{exp}	t_{avg} [sec]
F435W	10349	30	Globular Cluster	2	340
F435W	10524	7	Globular Cluster	2	300
F435W	10595	2	Globular Cluster	2	340
F435W	10595	7	Globular Cluster	2	340
F435W	9978	5e	Extragalactic Field	3	1220
F435W	15647	13	Extragalactic Field	2	720
F435W	9583	99	Extragalactic Field	2	1200
F435W	10584	13	Resolved Galaxy	2	600
F435W	10760	2	Resolved Galaxy	8	545
F435W	10760	4	Resolved Galaxy	8	543
F435W	12513	2	Resolved Galaxy	3	958
F435W	9490	a3	Resolved Galaxy	2	450
F606W	10146	3	Globular Cluster	2	1259
F606W	10146	4	Globular Cluster	2	1175
F606W	10775	ab	Globular Cluster	4	130
F606W	14164	1	Globular Cluster	3	353
F606W	10536	13	Extragalactic Field	2	347
F606W	13375	4	Extragalactic Field	3	818
F606W	13375	7	Extragalactic Field	3	803
F606W	13671	35	Extragalactic Field	3	400
F606W	10190	13	Resolved Galaxy	2	1200
F606W	10190	28	Resolved Galaxy	4	540
F606W	10260	5	Resolved Galaxy	3	790
F606W	10260	7	Resolved Galaxy	3	790
F606W	13057	1	Resolved Galaxy	2	346
F606W	14343	1	Resolved Galaxy	6	350
F814W	10775	29	Globular Cluster	4	150
F814W	10775	ad	Globular Cluster	4	150
F814W	12602	2	Globular Cluster	4	537
F814W	9405	4b	Extragalactic Field	4	400
F814W	9405	6d	Extragalactic Field	2	600
F814W	9450	14	Extragalactic Field	3	360
F814W	9450	16	Extragalactic Field	4	360
F814W	12058	1	Resolved Galaxy	3	502
F814W	12058	12	Resolved Galaxy	3	502
F814W	12058	16	Resolved Galaxy	3	502
F814W	14704	1	Resolved Galaxy	4	550
F814W	9490	a2	Resolved Galaxy	2	360

NOTE—Observation set ID is generally, but not always, equivalent to the HST phase-2 visit number

The data quality arrays are also directly derived from the extension of the exposure files. During the training process, the pixels flagged by the data quality arrays do not contribute to back-propagation nor model evaluation. We further used 7×7 ($0.35'' \times 0.35''$) dilation kernel to expand the saturation mask for pixels brighter than $70000 e^-$.

Finally, we use the module mentioned earlier, TWEAKREG to identify common sources and compute vertical and horizontal shifts. There are plenty of parameters of TWEAKREG bundled as `Imagefindpars`, which give users control over the algorithm that extracts sources from the image. Among them, there exist two parameters, `conv.width` and `threshold`, which are the convolution kernel width in pixels and the object detection threshold above the local background in units of sigma. These parameters were manually adjusted empirically for every image sets to minimize the horizontal and vertical root-mean-square error of the fit; refer to Table A1 for the full detail about the parameter choice. The resulting fit information is stored in the header of the exposure. Given the fit information, ASTRODRIZZLE aligns multiple exposures to combine them. Then, it computes the median images, which are compared against the single-exposure images to create CR masks. For further details about the ASTRODRIZZLE parameters used in the procedure, refer to Section 3 of Zhang & Bloom (2020).

The same procedure was repeated to build the test datasets. The observation sets that we used are given in Table 2. Individual models were tested with the respective test set using Receiver Operating Characteristic (ROC) curves, separately for the extragalactic field, globular cluster, to assess their performance on each field. The global model was tested with three individual test sets. For further detail about model testing, refer to Section 3.1

Table 2. HST ACS/WFC test dataset: 12 observation sets in total were used to test DEEPCR-ACS/WFC

Filter	Proposal ID	Observation Set ID*	Field Type	N_{exp}	t_{avg} [sec]
F435W	10120	3	Globular Cluster	3	340
F435W	11340	11	Globular Cluster	2	464
F435W	9694	6	Extragalactic Field	2	535
F435W	10342	3	Resolved Galaxy	2	680
F606W	11586	5	Globular Cluster	4	505
F606W	12438	1	Extragalactic Field	3	293
F606W	10407	3	Resolved Galaxy	3	1132
F606W	13364	95	Resolved Galaxy	2	565
F814W	12602	1	Globular Cluster	6	848
F814W	10092	1	Extragalactic Field	4	507
F814W	12058	6	Resolved Galaxy	3	502
F814W	13804	6	Resolved Galaxy	2	1341

3. RESULTS

3.1. Model Evaluation

We evaluated the models with a Receiver Operating Characteristic (ROC) curves. As it has been already proven that DEEPCR potentially outperforms LACOSMIC in Zhang & Bloom (2020), the ROC curve of LACOSMIC will not be displayed in this section. We plot the true positive rates (TPR; the model correctly identifying true CRs) against the false-positive rates (FPR; model identifying clean pixels as CRs) to visualize the test result.

The models are evaluated with two settings: with and without dilation kernel. With the dilation, the radius of prediction is expanded by 3×3 kernel; if any CR is present within the dilated area, the model is not penalized for false detection—analogue to shooting a bullet with a bigger caliber. Figure 3 shows ROC curves of DEEPCR-ACS/WFC and individual models, where the y-axis shows the TPR and the x-axis shows the FPR.

The dotted lines represent the ROC curves of the dilated models and clearly illustrate the effect of dilation, which brings up the TPR at fixed FPR. Overall, the global model and the individual model retain the original performance

Table 3. Performance comparison between DEEPCR-ACS/WFC and individual filter models on every field types (globular clusters, extragalactic fields, resolved galaxies). The models marked with the “+” sign indicates that the dilation kernel is utilized. For each entry, the TPR for corresponding FPR (0.05% and 0.5%) is shown.

Model	Globular Clusters		Extragalactic Fields		Resolved Galaxies	
	TPR (0.05%)	TPR (0.5%)	TPR (0.05%)	TPR (0.5%)	TPR (0.05%)	TPR (0.5%)
DEEPCR-ACS/WFC	80.24%	95.53%	87.47%	99.39%	76.46%	90.36%
DEEPCR-ACS/WFC F435W	78.38%	94.61%	86.26%	99.28%	75.86%	90.81%
DEEPCR-ACS/WFC +	92.06%	96.93%	98.63%	99.87%	89.95%	91.80%
DEEPCR-ACS/WFC F435W +	92.14%	96.13%	98.71%	99.84%	90.06%	92.39%
DEEPCR-ACS/WFC	85.98%	97.45%	89.08%	99.37%	64.79%	86.80%
DEEPCR-ACS/WFC F606W	85.32%	97.22%	88.64%	99.28%	60.73%	85.40%
DEEPCR-ACS/WFC +	95.52%	98.56%	95.97%	99.75%	82.53%	92.11%
DEEPCR-ACS/WFC F606W +	95.08%	98.45%	95.60%	99.67%	78.82%	91.69%
DEEPCR-ACS/WFC	82.53%	94.63%	92.00%	99.58%	67.01%	89.53%
DEEPCR-ACS/WFC F814W	83.75%	95.27%	91.44%	99.50%	66.12%	89.57%
DEEPCR-ACS/WFC +	94.37%	96.86%	98.31%	99.80 %	85.32 %	92.86%
DEEPCR-ACS/WFC F814W +	94.53%	97.07%	98.37%	99.86%	84.39%	92.82%

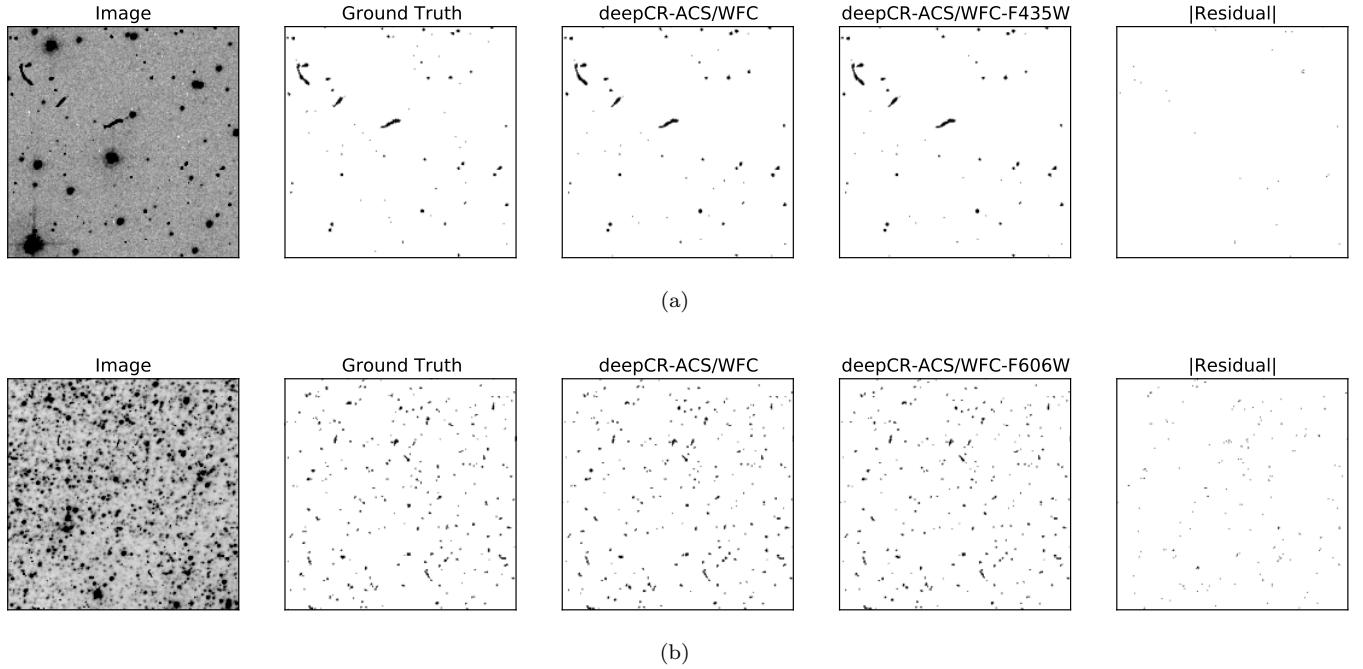


Figure 2. The same images as in Figure 1 were processed. (a) shows the raw original image taken with ACS/WFC F435W filter, the ground truth CR mask generated by ASTRODRIZZLE, mask predicted by the global model, mask predicted by the individual model, and the residual, defined by $|\text{mask}_{\text{global}} - \text{mask}_{\text{individ}}|$. (b) shows the same plots, but with a F606W image, and masks generated by the corresponding model. As expected, there is a minimal residual in the masks predicted for the sparsely populated image and relatively larger discrepancy for the densely populated image.

of the model presented in Zhang & Bloom (2020), achieving near 100% detection rates in extragalactic fields, $\sim 95\%$ in globular clusters, and $\sim 90\%$ in the resolved galaxies without dilation. At fixed FPR, it is shown that the orange curves (DEEPCR-ACS/WFC) and the black curves (individual models) give similar TPRs. Numerical values for the

TPRs at FPRs of 0.5% and 0.05% are shown in Table 3. In all cases, the global model yields comparable, if not better, TPRs compared to the individual models. Both the individual models and global model does not display a significant difference in performance, where the maximum discrepancy in TPR at FPR of 0.05% is $\sim \pm 1\%$. This result would be better understood with Figure 2. In the sparse (in other words, *easy*) fields, it is expected that both the models will perform similarly, which justifies the minimal residual in Figure 2.(a). In denser fields, the gap in performance is expected since their images are more difficult to align, and producing reliable CR masks is tricky. However, given the density of true CRs, there is still minimal residual appearing in Figure 2.(b), which suggests that the global model functions as well as the individual models. To reproduce the test results and the plots, refer to Appendix B.

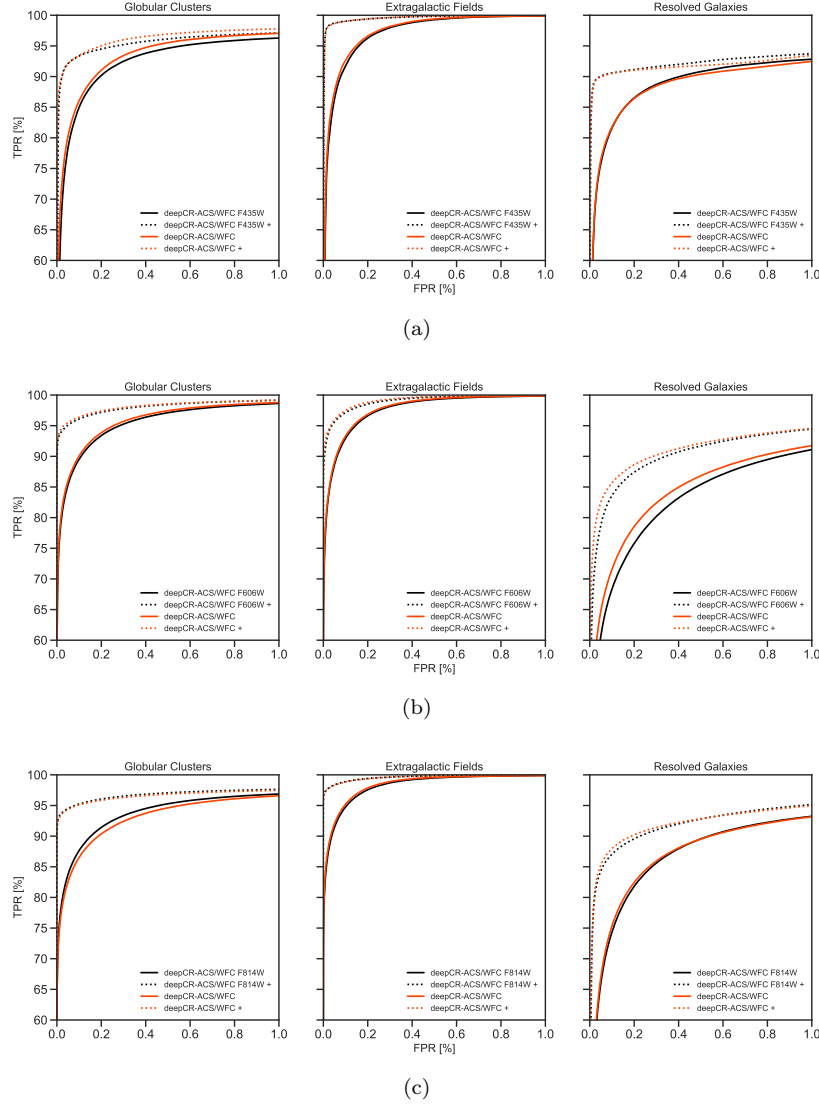



Figure 3. The ROC curves of DEEPCR-ACS/WFC (the global model) and individual models, tested with corresponding test datasets; (a), (b) and (c) show the ROC curves of the F435W, F606W, and F814W models respectively, along with the global model. The models are evaluated on three different fields—globular clusters, extragalactic fields, and resolved galaxies—and the results are shown in the first, second, and third columns, respectively. The x-axis denotes the false positive rate (%), and the y-axis shows the true positive rate (%). The testing result with dilation kernel is marked with the “+” sign in the legends.

3.2. Usage

The models are implemented in Python and is available in GitHub repository [deepCR](#) . The individual as models and the global model are available as ACS-WFC-F435W-2-32, ACS-WFC-F606W-2-32, ACS-WFC-F814W-2-32, and ACS-WFC-2-32. Note that the global `inpaint` model is currently not available, because current package does not support `inpaint` model training. However, we aim to release the `inpaint` model as a next step. We anticipate that the ACS-WFC-F606W-2-32 `inpaint` model will be sufficient for lower/higher wavelength ranges.

```
from deepCR import deepCR
global_md1 = deepcr(mask="ACS-WFC-2-32",
                    inpaint="ACS-WFC-F606W-2-32",
                    device="GPU")
mask, cleaned_image = mdl.clean(image)
```

4. CONCLUSION

The HST ACS/WFC F606W model presented in [Zhang & Bloom \(2020\)](#) demonstrated its potential in outperforming LACOSMIC. Although the original model was expected to maintain its performance in wider wavelength ranges, we further reinforced the anticipation by training new models with images from HST ACS/WFC F435W, F606W, F814W filters. As suggested in [3](#), the newly developed individual models trained with HST ACS/WFC F435W, F606W, and F814W data retained the performance of the original model in [Zhang & Bloom \(2020\)](#), showing $\sim 100\%$, $\sim 95\%$, and $\sim 90\%$ TPRs in extragalactic field, globular cluster and resolved galaxy images, respectively. Further, the *all-in-one* global model, DEEPCR-ACS/WFC, was also developed to ameliorate the applicability of the model. The global model was tested with the F435W, F606W, F814W test datasets separately and demonstrated that it is a sufficient substitute for the individual models, with a maximum $\sim \pm 1\%$ difference in FPR of 0.05%.

We intend to expand the scope of the model from photometry to spectroscopy. In light of recently commissioned Dark Energy Spectroscopic Instrument (DESI) survey ([Martini et al. 2018](#); [Zhou et al. 2020](#)), we expect the spectroscopic model will significantly aid the data preprocessing, given the promising detection rates demonstrated in [Section 3](#) and the speed superiority ([Zhang & Bloom 2020](#)) over LACOSMIC. Furthermore, as stated in [Section 3.2](#), we plan to implement `inpaint` model training and release the global `inpaint` model for HST ACS/WFC.

Software: ASTROPY ([Astropy Collaboration et al. 2018](#)), ASTRODRIZZLE ([Hack et al. 2012](#)), TWEAKREG ([Gonzaga & et al. 2012](#)), NUMPY ([Harris et al. 2020](#)), MATPLOTLIB ([Hunter 2007](#)), SCIKIT-IMAGE ([van der Walt et al. 2014](#)), ASTROCRAPPY ([van Dokkum 2001](#)), SCIPY ([Virtanen et al. 2020](#)), PYTORCH ([Paszke et al. 2019](#)), JUPYTER ([Kluyver et al. 2016](#))

APPENDIX

A. TWEAKREG PARAMETERS

Table A1. TWEAKREG parameters to align exposure images.

Filter	Proposal ID	Observation Set ID	Field Type	conv.width	threshold
F435W	10349	30	Globular Cluster	3.5	11785
F435W	10524	7	Globular Cluster	3.5	8785
F435W	10595	2	Globular Cluster	3.5	6500
F435W	10595	7	Globular Cluster	3.5	11500
F435W	10120	3	Globular Cluster	3.5	2085
F435W	11340	11	Globular Cluster	3.5	14185

Table A1 continued on next page

Table A1 (*continued*)


Filter	Proposal ID	Observation Set ID	Field Type	conv_width	threshold
F435W	15647	13	Extragalactic Field	6.0	950
F435W	9583	99	Extragalactic Field	6.0	300
F435W	9978	5e	Extragalactic Field	6.0	800
F435W	9694	6	Extragalactic Field	6.0	1000
F435W	10584	13	Resolved Galaxy	3.5	400
F435W	10760	2	Resolved Galaxy	3.5	800
F435W	10760	4	Resolved Galaxy	3.5	400
F435W	12513	2	Resolved Galaxy	3.5	400
F435W	9490	a3	Resolved Galaxy	3.5	400
F814W	9490	a2	Resolved Galaxy	3.5	1500
F435W	10342	3	Resolved Galaxy	3.5	200
F606W	10146	3	Globular Cluster	3.5	300
F606W	10146	4	Globular Cluster	3.5	2839
F606W	14164	1	Globular Cluster	3.5	11785
F606W	11586	5	Globular Cluster	3.5	11050
F606W	10775	ab	Globular Cluster	3.5	3785
F606W	10536	13	Extragalactic Field	6.0	500
F606W	13375	4	Extragalactic Field	6.0	1250
F606W	13375	7	Extragalactic Field	6.0	280
F606W	13671	35	Extragalactic Field	6.0	200
F606W	12438	1	Extragalactic Field	6.0	300
F606W	13057	1	Resolved Galaxy	3.5	1150
F606W	14343	1	Resolved Galaxy	3.5	800
F606W	10407	3	Resolved Galaxy	3.5	900
F606W	10190	13	Resolved Galaxy	3.5	400
F606W	10190	28	Resolved Galaxy	3.5	300
F606W	10260	5	Resolved Galaxy	3.5	150
F606W	10260	7	Resolved Galaxy	3.5	600
F606W	13364	95	Resolved Galaxy	3.5	120
F814W	10775	29	Globular Cluster	3.5	1900
F814W	10775	ad	Globular Cluster	3.5	3000
F814W	12602	2	Globular Cluster	3.5	7000
F814W	12602	1	Globular Cluster	3.5	6000
F814W	9405	4b	Extragalactic Field	6.0	500
F814W	9405	6d	Extragalactic Field	6.0	500
F814W	9450	14	Extragalactic Field	6.0	100
F814W	9450	16	Extragalactic Field	6.0	300
F814W	10092	1	Extragalactic Field	6.0	300
F814W	12058	1	Resolved Galaxy	3.5	800
F814W	12058	12	Resolved Galaxy	3.5	500
F814W	12058	16	Resolved Galaxy	3.5	1200

Table A1 *continued on next page*

Table A1 (*continued*)

Filter	Proposal ID	Observation Set ID	Field Type	conv_width	threshold
F814W	14704	1	Resolved Galaxy	3.5	400
F814W	12058	6	Resolved Galaxy	3.5	400
F814W	13804	6	Resolved Galaxy	3.5	400

B. REPRODUCTION

We have published a GitHub repository `deepCR-ACS-WFC-reproduction` , which contains `deepCR-ACS-WFC.py`. When executed, the script downloads the processed training and test data, train the individual and global models, and run model testing. For optimal execution, ~ 60 GB of disk space is required, and GPU support is desired.

REFERENCES

- Astropy Collaboration, Price-Whelan, A. M., SipHocz, B. M., et al. 2018, *aj*, 156, 123, doi: [10.3847/1538-3881/aabc4f](https://doi.org/10.3847/1538-3881/aabc4f)
- Farage, C. L., & Pimblet, K. A. 2005, *PASA*, 22, 249, doi: [10.1071/AS05012](https://doi.org/10.1071/AS05012)
- Freudling, W. 1995, *Publications of the Astronomical Society of the Pacific*, 107, 85, doi: [10.1086/133519](https://doi.org/10.1086/133519)
- Fruchter, A. S., & Hook, R. N. 2002, *PASP*, 114, 144, doi: [10.1086/338393](https://doi.org/10.1086/338393)
- Gonzaga, S., & et al. 2012, *The DrizzlePac Handbook*
- Hack, W. J., Dencheva, N., Fruchter, A. S., et al. 2012, in *American Astronomical Society Meeting Abstracts*, Vol. 220, American Astronomical Society Meeting Abstracts #220, 135.15
- Harris, C. R., Millman, K. J., van der Walt, S. J., et al. 2020, *Nature*, 585, 357, doi: [10.1038/s41586-020-2649-2](https://doi.org/10.1038/s41586-020-2649-2)
- Hunter, J. D. 2007, *Computing in Science & Engineering*, 9, 90, doi: [10.1109/MCSE.2007.55](https://doi.org/10.1109/MCSE.2007.55)
- Kluyver, T., Ragan-Kelley, B., Pérez, F., et al. 2016, in *Positioning and Power in Academic Publishing: Players, Agents and Agendas*, ed. F. Loizides & B. Schmidt (Netherlands: IOS Press), 87–90. <https://eprints.soton.ac.uk/403913/>
- Martini, P., Bailey, S., Besuner, R. W., et al. 2018, in *Society of Photo-Optical Instrumentation Engineers (SPIE) Conference Series*, Vol. 10702, *Ground-based and Airborne Instrumentation for Astronomy VII*, ed. C. J. Evans, L. Simard, & H. Takami, 107021F, doi: [10.1117/12.2313063](https://doi.org/10.1117/12.2313063)
- Paszke, A., Gross, S., Massa, F., et al. 2019, in *Advances in Neural Information Processing Systems* 32, ed. H. Wallach, H. Larochelle, A. Beygelzimer, F. d'Alché-Buc, E. Fox, & R. Garnett (Curran Associates, Inc.), 8024–8035. <http://papers.neurips.cc/paper/9015-pytorch-an-imperative-style-high-performance-deep-learning-library.pdf>
- Pych, W. 2004, *PASP*, 116, 148, doi: [10.1086/381786](https://doi.org/10.1086/381786)
- Rhoads, J. E. 2000, *PASP*, 112, 703, doi: [10.1086/316559](https://doi.org/10.1086/316559)
- van der Walt, S., Schönberger, J. L., Nunez-Iglesias, J., et al. 2014, *PeerJ*, 2, e453, doi: [10.7717/peerj.453](https://doi.org/10.7717/peerj.453)
- van Dokkum, P. G. 2001, *PASP*, 113, 1420, doi: [10.1086/323894](https://doi.org/10.1086/323894)
- Virtanen, P., Gommers, R., Oliphant, T. E., et al. 2020, *Nature Methods*, 17, 261, doi: [10.1038/s41592-019-0686-2](https://doi.org/10.1038/s41592-019-0686-2)
- Zhang, K., & Bloom, J. S. 2020, *ApJ*, 889, 24, doi: [10.3847/1538-4357/ab3fa6](https://doi.org/10.3847/1538-4357/ab3fa6)
- Zhou, R., Newman, J. A., Dawson, K. S., et al. 2020, *Research Notes of the American Astronomical Society*, 4, 181, doi: [10.3847/2515-5172/abc0f4](https://doi.org/10.3847/2515-5172/abc0f4)